Journal of Hazardous Materials 453 (2023) 131331

Contents lists available at ScienceDirect

Journal of Hazardous Materials

journal homepage: www.elsevier.com/locate/jhazmat

Research Paper

The impact of metallic nanoparticles on gut fermentation processes: An integrated metabolomics and metagenomics approach following an *in vitro* digestion and fecal fermentation model

Filippo Vaccari [a,1], Leilei Zhang [a,1], Gianluca Giuberti [a,*], Alfina Grasso [b], Francesca Bandini [a], Pascual García-Pérez [a,d], Chiara Copat [b], Luigi Lucini [a], Margherita Dall'Asta [c], Margherita Ferrante [b], Edoardo Puglisi [a]

[a] Department for Sustainable Food Process, Università Cattolica del Sacro Cuore, Piacenza, Italy
[b] Department of Medical, Surgical Sciences and Advanced Tehnologies Università degli studi di Catania, Piazza dell'Università 2, 95131 Catania, Italy
[c] Department of Animal Science, Food, and Nutrition, Università Cattolica del Sacro Cuore, Piacenza, Italy
[d] Nutrition and Bromatology Group, Analytical and Food Chemistry Department, Faculty of Food Science and Technology, Univesidade de Vigo, Ourense Campus, 32004 Ourense, Spain

HIGHLIGHTS

- Ag and ZnO increased relative *E. coli* and *B.vulgatus* abundance and proteolytic activity.
- Low concentrations of TiO_2 and Ag, increased relative *E.* coli abundance and proteolytic activity.
- Low concentrations of TiO_2 reduced *B. longum* relative abundance.
- TiO_2 treatment manifested a pro-inflammatory reaction.
- Low concentration of Ag and ZnO had a pronounced impact on microbiome and metabolome.

GRAPHICAL ABSTRACT

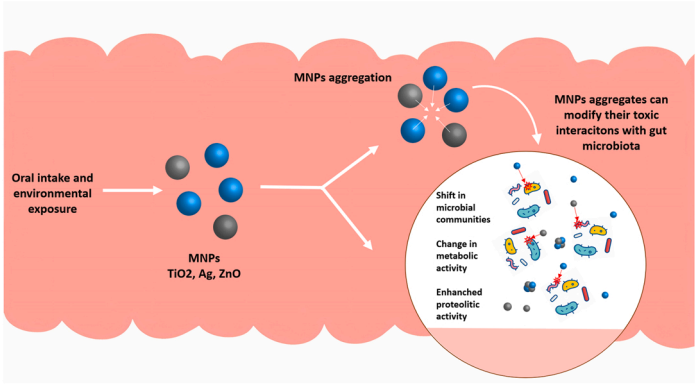

ARTICLE INFO

Editor: Dr. S. Nan

Keywords:
Human gut microbiome
Human gut metabolome
Titanium dioxide
Zinc oxide
Silver

ABSTRACT

Metallic nanoparticles (MNPs) are becoming widespread environmental contaminants. They are currently added to several food preparations and cause a fast-growing concern for human health. The present work aims to assess the impact of zinc oxide (ZnO), titanium dioxide (TiO_2), and silver (Ag) nanoparticles (NPs) on the human gut metabolome and microbiome. Water samples spiked with two different concentrations of each MNPs were subjected to *in-vitro* gastrointestinal digestion and *in-vitro* large intestine fermentation. The effects of the treatments were determined through 16 S amplicon sequencing and untargeted metabolomics. Multi-omics data integration was then applied to correlate the two datasets. MNPs treatments modulated the microbial genera

* Corresponding author.
E-mail address: gianluca.giuberti@unicatt.it (G. Giuberti).
[1] These two authors contributed equally to this work.

https://doi.org/10.1016/j.jhazmat.2023.131331
Received 15 November 2022; Received in revised form 28 March 2023; Accepted 29 March 2023
Available online 30 March 2023

Bifidobacterium, *Sutterella*, *Escherichia* and *Bacteroides*. The treatments, especially the lower concentrations of Ag and ZnO, caused modulation of indole derivatives, peptides, and metabolites related to protein metabolism in the large intestine. Notably, these metabolites are implicated in ulcerative colitis and inflammatory bowel disease. TiO_2 NPs treatment in all concentrations increased *E.coli* relative abundance and decreased the abundance of *B. longum*. Moreover, for TiO2, an enrichment in proinflammatory lipid mediators of arachidonic acid metabolites, such as prostaglandin E2 and leukotrienes B4, was detected. For all metals except TiO_2, low NP concentrations promoted differentiated profiles, thus suggesting that MNPs aggregation can limit adverse effects on living cells.

1. Introduction

Human exposure to metal nanoparticles (MNPs) can derive from multiple sources such as pharmaceuticals, medicine, electronics, and the textile industry. At the end of their life cycle, MNPs can accumulate in the environment, thus posing a severe environmental threat. A wide range of studies has shown that metal oxide nanoparticles (NPs) can also cause toxic effects on plants, algae, bacteria, fish, and mammalian cells [67]. The consequences of the wide usage and disposal of NPs can already be observed in aquatic environments, and processes of MNP bioaccumulation have been studied in seafood products [25–27]. Titanium dioxide (TiO_2), silver (Ag), and zinc oxide (ZnO) MNPs are among the most common nano-metals commercially used in the food industry and are now increasingly used as a nano drug delivery system, especially in combination with antibiotic treatments, to reduce the risk of microbial resistance [30]. One of the major sources of human intake as well as a recent cause of concern for public health is the introduction of NPs through the oral route. Commercial TiO_2 (E171) is a mixture of different-sized particles, of which approximately 50% are < 100 nm in diameter. TiO_2 is directly added to many foods, such as bakery wares, soups, broths, and sauces, as a colorant and biocidal. The daily TiO_2 NP exposure in Europe has been estimated to be 1.9–11.5 mg/kg body weight (BW) for toddlers and 0.9–12.8 mg/kg BW for children [70]. However, the real exposure could be much greater due to the increased use of NPs as additives in food packaging and their presence in the environment. On May 6th, 2021, the European Food Safety Authority (EFSA) safety assessment reported that TiO_2 could no longer be regarded as a safe food additive [70] due to a concern about genotoxicity. Consequently, a ban on TiO_2 as a food additive in the EU was approved by state members. However, TiO_2 is still commonly used in many countries as a food additive, and food packaging systems currently utilize this nanomaterial [23]. Ag (E174) is mainly used in the food industry as a colorant and antimicrobial. In commercial nanoparticular form, 97% of the particles have a < 100 nm diameter, and most are < 40 nm in diameter [17]. Ag NPs are present in some commercial products, either as part of food packaging materials or as an ingredient in foods, particularly dietary supplements, breath-freshening microsweets, and bakery goods. Population groups with the highest exposure to Ag are children and adolescents with a medium intake ranging from 0.10 to 2.6 mg/kg BW [59]. ZnO is listed as a generally recognized safe ingredient by the Food and Drug Administration, and its NPs are frequently used in antimicrobial food packaging. The average particle size of ZnO powder in nanoform is between 30 nm and 60 nm, and 1% of the particles are smaller than 30 nm. EFSA has assessed exposure levels for ZnO as < 25 mg [57].

MNPs can be transferred from packaging materials to food, resulting in direct oral human exposure [71,72]. Depending on the characteristics of the plastic polymer harboring the nanometals, the nature of the NPs, and the physical characteristics of the food product being conserved, the efficiency of NP migration can be affected. For example, a low pH in the food matrix enhances Ag NP migration from a package to the food matrix [1]. Concerning their fate in the human body, nanometals exert an effect through their derived ions, which are released when nanometals are dissolved in an aqueous medium or as a direct consequence of their physical structure [67]. MNPs have also been observed to modify gastrointestinal tract (GIT) homeostasis, as they negatively impact mucus-producing goblets and other intestinal epithelial cells [28]. Furthermore, the stability, aggregation, and physical characteristics of MNPs are influenced by interactions with the GIT: this has been observed for peristalsis, pH, gastric enzymes, food composition, endogenous biochemicals, and commensal microbes [8]. Moreover, the effect of prolonged exposure to MNPs has been researched regarding inflammatory bowel disease (IBD), coeliac disease (CD) and ulcerative colitis (UC), and this research suggest that there is a possibility that these NPs exacerbate or even trigger the symptoms of these diseases [39,41]. Coeliac disorder patients have also shown an altered gut microbiome before disease progression [49], which implies that the gut microbiome has a direct effect on the pathogenesis of CD.

The present work aimed to assess the impact of three different MNPs: ZnO, TiO_2 and Ag by monitoring both gut metabolome and microbiome after an *in-vitro* human digestion procedure, thus further clarifying the effects of these compounds on the GIT. The digestion was carried out using different gastrointestinal fluids simulators. Subsequently, an *in-vitro* large intestine fermentation was performed using feces obtained by pooling equal amounts of human fecal samples. Given the limited knowledge available, high-throughput sequencing and metabolomics were chosen to profile bacterial communities and metabolites after large intestine fermentation according to a hypothesis-free untargeted approach. Moreover, the datasets obtained from metabolomics and 16 S amplicon sequencing analysis were subsequently integrated to perform a multi-omics data fusion interpretation aimed at comprehensively unraveling the effect of nanomaterials on digestion processes.

2. Materials and methods

2.1. Sample preparation and in-vitro digestion and fermentation

Water samples were spiked with two different concentrations (Table 1) of each of the three MNPs and subjected to *in-vitro* digestion. Spiking was done from Ag-NPs standard (PELCO® 40 nm, Citrate, NanoXactTM, Ted Pella Inc.), TiO_2-NPs standard (TiO_2 Nano Powder 60 nm, Rutile, 99.9%, AEM) and ZnO-NPs standard (ZnO-NPs nano powder 30 nm, AEM®, purity 98.8%, Changsha, Hunan, China), purchased from Nanovision (Brugherio, MB, Italy). The low concentration, which was based on the average MNPs concentration previously quantified in seafood products, was used to estimate the effects of actual concentrations that naturally occur in foods [25–27], while the high concentration was chosen to investigate the effect of a large level of exposure on the gut microbiome and metabolic profile.

Table 1
Table reporting added nanoparticles, and their size and concentration measured with Inductively Coupled Plasma Mass Spectrometry (ICP-MS) after spiking.

Particle	*Diameter of the particle (nm)*	*Conc. 1 (mg/mL)*	*Part. mL*	*Conc. 2 (mg/mL)*	*Part. mL*
TiO_2	60	0.41	8.4×10^5	1.1	2.4×10^6
Ag	40	0.002	2.4×10^4	0.02	1.7×10^5
ZnO	30	0.001	1.3×10^4	0.01	1.1×10^5

All samples were subjected to an *in-vitro* digestion process followed by an *in-vitro* fecal fermentation to mimic the physiological processes in the human gut. Aqueous samples were first subjected to the standardized three-step static *in-vitro* human gastro-intestinal digestion model proposed by Minekus et al. [45]. The procedure is based on the sequential simulation of the oral, gastric, and intestinal adult digestion phases. During each step, the substrate was incubated for a specific time and subjected to key physiological conditions using simulated salivary fluid (SSF), simulated gastric fluid (SGF), and simulated intestinal fluid (SIF) [45]. The extended protocol is described elsewhere [45]. The oral phase involved the SSF (1:1 w/v) with α-amylase from human saliva (SKU code: A1031; Sigma-Aldrich; 75 $U{\cdot}mL^{-1}$) was kept at 37 °C for 2 min. After this passage, the samples were diluted with 10 mL of SGF (pH 3.0) containing pepsin (SKU code: P7012; Sigma-Aldrich; 2.000 $U{\cdot}mL^{-1}$) at 37 °C for 120 min. The gastric chime was then diluted with 20 mL of SIF (pH = 7.0) containing bile salts (SKU code: B8631; Sigma-Aldrich; 10 mM) and pancreatin (SKU code: P7545; Sigma-Aldrich; 100 $U{\cdot}mL^{-1}$ based on trypsin activity) for 120 min. During the *in-vitro* digestion, appropriate amounts of HCl (1 M) and NaOH (1 M) were added for pH adjustment. The *in-vitro* gastro-intestinal digestion was stopped through ice bath cooling. Afterwards, the *in-vitro* digested residues were directly subjected to an *in-vitro* large intestine fermentation, as detailed by Pérez-Burillo et al. [51]. Feces were collected from three healthy adults who were not treated with antibiotics. Freshly voided fecal samples were captured after defecation, and the samples were immediately stored in an anaerobic jar and processed within 20 min of collection. The CO_2-saturated fermentation medium contained 0.05 g mL^{-1} of fresh feces obtained by pooling equal amounts (wet weight) of feces from each subject. Sample manipulation and incubation were carried out under continuous CO_2 flushing (technical grade: 5.5; SAPIO, Monza, Italy). The fecal samples were then processed and incubated in glass vessels for the *in-vitro* fermentation step which lasted 20 h and was maintained at 37 °C under gentle oscillation as proposed by [51]. Samples were then immersed in ice to stop the reactions and centrifuged at 10,000g for 12 min to remove insoluble particulate. Supernatants were collected and stored at − 4 °C for analysis. An informed written consent was obtained from all subjects, and the study was conducted in conformity with the Helsinki Declaration. The Ethics Committee "Comitato Etico dell'Area Vasta Emilia Nord" approved the study (767/2021/TESS/AUSLPC).

2.2. 16S amplicon sequencing and PICRUSt2 predictive analysis

Microbiological analyses were carried out on samples after the anaerobic fermentation phase. Total genomic DNA was extracted using FastDNA™ SPIN Kit for Soil, according to the manufacturer's protocol. Extracted DNA was quantified using a Quant-iTTM HS ds-DNA assay kit (Invitrogen, Paisley, UK) with a QuBit 2.0 fluorometer (Invitrogen, Paisley, UK).

High-throughput sequencing of 16 S rDNA for bacterial communities was performed on both MNP-spiked and control samples. Hypervariable region V3-V4 of the bacterial 16 S rDNA gene was amplified by PCR to analyse bacterial diversity. The universal primers 343 f (5′-TACGGRAGGCAGCAG-3′) and 802r (5′- TACNVGGGTWTCTAATCC-3′) were used. The reaction mix was composed of 12.5 μL of Phusion Flash High-Fidelity Master Mix (Thermo Fisher Scientific, Inc., Waltham, MA, USA), 1.25 μL of forward and reverse primers (10 μM), 1 ng of DNA template, and nuclease-free water for a final volume of 25 μL. The thermal cycle used for the amplification was the following: initial denaturation at 95 °C for 5 min, followed by 20 cycles of denaturation at 95 °C for 30 s, annealing at 50 °C for 30 s, an extension at 72 °C for 30 s and a final extension at 72 °C for 10 min. To sequence multiple samples in a single run a nested PCR, in which first-step products were used as a template for the second PCR step, was used [10]. Forward primers of the second PCR were indexed with a 9 nucleic acid-base extension at their 5′ as described by Fontana et al. [21,66]. Thermal profiles remained unchanged from the first step, while the number of cycles for the second amplifications corresponded to 10 cycles. Products from the second amplification step were multiplexed as a single pool using an equivalent molecular weight of 20 ng. To purify the pool, a solid phase reversible immobilization (SPRI) method (Agencourt AMPure XP kit; REF A63880, Beckman Coulter, Italy) was used. The sequencing process was performed by Novogene UK (Cambridge, UK), using the TruSeq DNA sample preparation kit (REF 15026486, Illumina Inc, San Diego, CA, USA) for amplicon library preparation. The Novaseq 6000 Illumina instrument (Illumina Inc, San Diego, CA, USA) obtained 250 bp paired-end reads. Illumina barcode demultiplexing and base calling were performed with the MiSeq Control Software version 2.3.0.3, RTA v1.18.42.0 and CASAVA v1.8.2 [13]. Raw sequences were aligned with the 'pandaseq' script [5] with a minimum overlap of 30 bp between read pairs and a maximum of two mismatches allowed, because V3–V4 16 S rDNA amplicons length is less than 500 bp, requiring 300 bp paired-end reads to reconstruct the full region. Sequences were subsequently demultiplexed according to sample indexes and primers by Fastx-toolkit Chimeras, homopolymers > 10 bp, sequences outside target regions, and non-targeted taxa were excluded according to [13]. Operational taxonomic units (OTU) and taxonomy-based statistical analysis were performed on the sequences. OTUs and taxonomy matrixes were generated with Mothur V1.32.1 [58], and statistical analysis was performed with R (http://www.R-project.org/) supplemented with Vegan package [19]. Taxonomy-based analyses were performed in Mothur with a minimum OTU length of 120. The statistical analyses performed were hierarchical clustering with the average linkage algorithm at different taxonomic levels [42,52], principal component analysis (PCA) for unconstrained groups and canonical correspondence analysis (CCA) for distance-based redundancy analysis [21].

In addition, the α diversity of the samples was calculated by analysing OTU- and taxonomy-based matrixes in R. To properly estimate any significative differences between different treatments, α diversity analysis based on sobs, and Observed Richness (S), on bacterial and fungal communities was run. Good's coverage [24] was used to assess the percentage diversity that emerged from sequencing. LSD pairwise comparison test ($\alpha < 0.05$) was used to assess significant differences. To identify significantly different OTUs between treatments, Metastats coupled to the paul FDR test for comparison of means was applied [50]. Analysis of variance of means (ANOVA) and Tukey's HSD pairwise comparison test ($\alpha < 0.05$) was performed to assess significant differences between samples. After amplicon sequencing analyses, samples were processed *via* Phylogenetic Investigation of Communities by Reconstruction of Unobserved States (PICRUSt2; https://github.com/picrust/picrust2; Version 2.5.1) to predict the putative metagenomic profile based on OTU abundances. PICRUSt2 uses the specific 16S-seq abundances to infer enzyme and metabolic abundances in each sample. The predicted functional characteristics were evaluated using the Kyoto Encyclopedia of Genes and Genomes database (KEGG; http://www.genome.jp/kegg/). All the pathways were indicated in MetaCyc format [15]. The results of PICRUSt2 predictions were analyzed using Statistical Analyzer of Metagenomic Profiles (STAMP 2.3.1: https://beikolab.cs.dal.ca/software/STAMP).

2.3. Metabolomic analysis

The anaerobically fermented samples were centrifugated at 5000 g for 10 min at 4 °C and further filtered through 0.22 μm cellulose syringe filters in ultra-high-pressure liquid chromatography (UHPLC) vials ready for analysis. The untargeted metabolomic analysis was carried out through a high-resolution mass spectrometry approach (HRMS) using a Q Exactive™ Focus Hybrid Quadrupole-Orbitrap Mass Spectrometer (Thermo Scientific, Waltham, MA, USA) coupled to a Vanquish ultra-high-pressure liquid chromatography (UHPLC) pump *via* a HESI-II probe (Thermo Scientific, USA), as previously described [53]. The chromatographic separation was performed using a Waters BEH C18

column (2.1 × 100 mm, 1.7 μm), applying a gradient from 6% to 94% of acetonitrile in 35 min, acidified with 0.1% formic acid in both phases (LC-MS grade, Carlo Erba Reagents S.r.l., Milan, Italy) [53]. The acquisition was performed using the positive ionization with a mass resolution of 70,000 at *m/z* 200, in full scan 100–1200 *m/z* with an injection volume of 6 μL. The automatic gain control target (AGC target) and the maximum injection time (IT) were 1e6 and 100 ms, respectively. Additionally, randomized injections of pooled quality control (QC) samples were performed in a data-dependent (Top N = 5) MS/MS mode with full scan mass resolution reduced to 17,500 at *m/z* 200, with an AGC target value of 1e5, maximum IT of 100 ms, and isolation window of 1.0 *m/z*, respectively.

The raw data (. RAW files) were processed through MS-DIAL software version 4.80; [65], and the annotation was performed *via* spectral matching against the comprehensive FooDB database [53]. Compounds annotation was defined with a tolerance for mass accuracy of 5 ppm with a level 2 of confidence in annotation, typical for untargeted metabolomics experiments, according to Metabolomics Standards Initiative (MSI). Only the featuring compounds annotated at MS/MS level were retained for multivariate statistical analysis. The metabolomics analysis was performed using the Agilent Mass Profile Professional B.15.1 (Agilent Technologies, Stevens Creek Blvd, Santa Clara, CA, USA) software for annotation and filtering as previously indicated [54,55]. Therein, an unsupervised multivariate hierarchical cluster analysis (HCA) was performed to evaluate the similarities and dissimilarities for all the treatments as a function of their metabolomic profile (Euclidean distance, Ward's linkage rule). Later, a Chemical Similarity Enrichment Analysis for Metabolomics (ChemRICH, available at chemrich.fiehnlab.ucdavis.edu) was performed to define the statistically enriched chemical composition according to the different treatments, compared to the control [6]. Specifically, significantly differential compounds reported by ANOVA analysis ($p < 0.05$, Bonferroni multiple testing correction) presenting fold change analysis > 2 (FC>2) were considered [6]. Finally, a supervised multivariate orthogonal projection to latent structures discriminant analysis (OPLS-DA) was carried out by the SIMCA v. 16.0.2 software (Umetrics, Malmo, Sweden), selecting variable importance in projection (VIP) compounds having a VIP score $>$ 1.2. The OPLS supervised modeling was validated through CV-ANOVA ($p < 0.01$) and overfitting was excluded by permutation testing ($n = 200$).

2.4. Multi-omics data integration

The outputs obtained from metabolomics and 16 S amplicon sequencing analysis were centered, and natural log of that ratio was transformed. The integration of two datasets was carried out using the

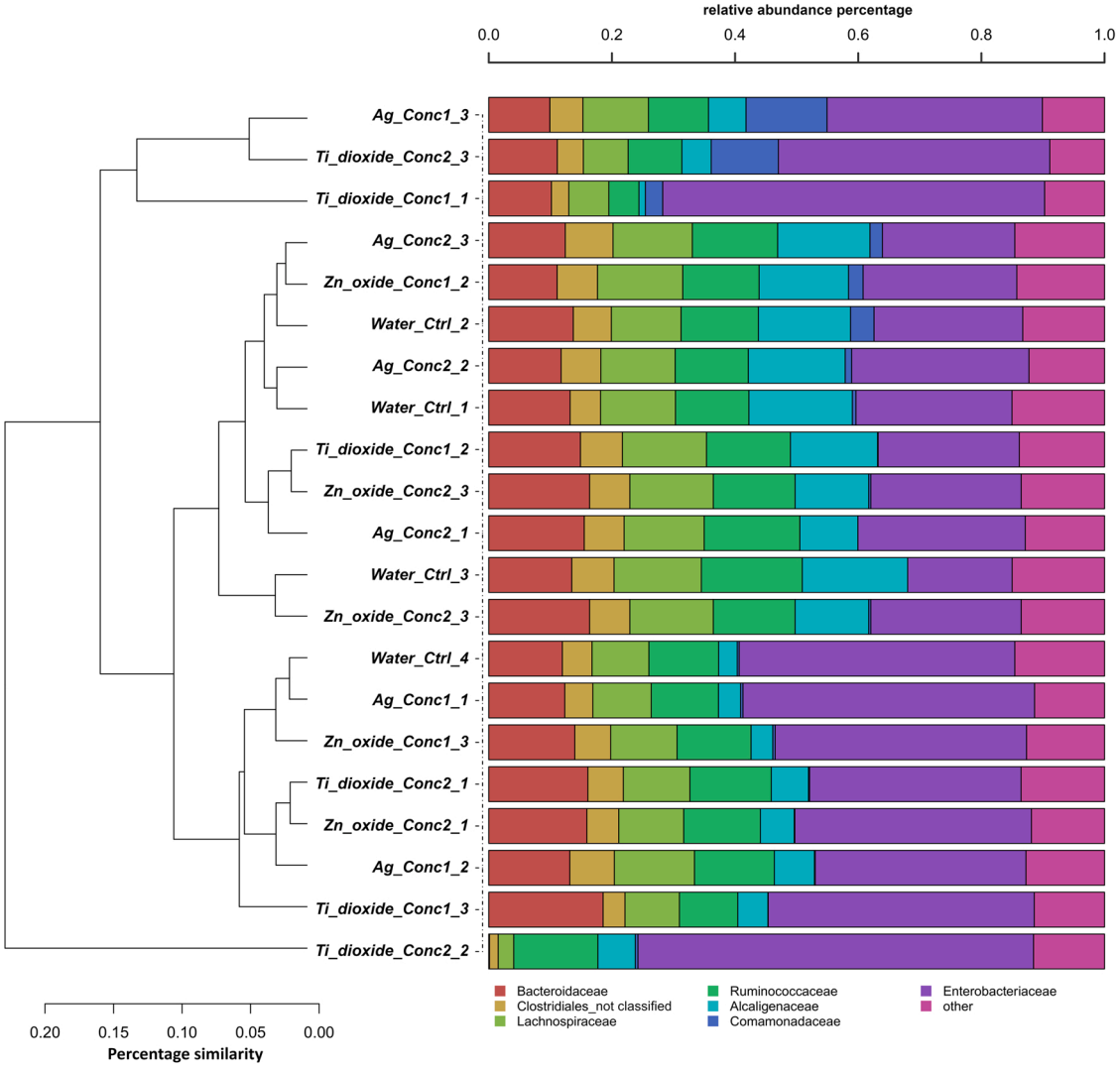

Fig. 1. A Hierarchical clustering of classified sequences using the average linkage algorithm according to the family classification for taxa contributing at ≥ 5% in at least one sample. Taxa with lower thresholds were added to the "other" sequence group.

DIABLO framework, a method for multi-omics classification and integration, in the mixOmics R package version 6.20.0 (http://mixomics.org/) [56]. The assessment of the correlation structure was carried out at the component level for each treatment. The optimal number of principal components and variables selected for the analysis were defined using the tuning function. Specifically, the number of components that achieves the best performance was chosen based on the balanced error rate (BER). In contrast, the variables number was determined through repeated and stratified cross-validation analysis to compare the performance of models constructed using different $\ell 1$ penalties.

3. Results

3.1. 16S amplicon sequencing and PICRUSt2 predictive analysis

Taxonomical assignment showed that 99.5% of sequences were correctly classified at the class level, whereas 99.4%, 93.8%, and 88.4% were correctly classified at the order and family and genus levels, respectively. The percentage at the species level was low, being 57%. Fig. 1. shows the most abundant families: there was a 93.4% coverage among samples of water spiked with ZnO, TiO_2, Ag and plan sterilized water (negative control), with a hierarchical clustering showing a general homogeneity among treatments and controls. A consistent relative abundance of families was observed at the taxonomical level and macroscopic level: *Enterobacteriaceae, Bacteroidaceae, Lachnospiraceae,* and *Ruminococcaceae*.

An OTU-based approach was performed for each NP to evaluate the total bacterial communities. Fig. 2. shows a Metastats model employed to evaluate the effect of single MNPs on the relative abundances of OTUs comprising 95% of the bacterial diversity. The taxonomy of the most abundant OTUs, which was assigned using the Ribosomal Database Project, reached the species level in most cases. For each OTU, treatment bars followed by different letters indicate a significant difference in relative abundance (Tukey's test; $P < 0.05$). The genera *Escherichia*, *Sutterella* and *Bacteroides* were most frequently observed in both negative and spiked samples. OTUs belonging to species *E. coli* were classified in all samples as the relatively most abundant. The presence of nanometals, particularly Ag and TiO_2, in the least concentrated treatments resulted in a significant increase of *E. coli* relative abundance. The *Sutterella* genus was found to be significantly modulated by MNPs: in particular, *Sutterella wadsworthensis* was detected at different abundances in all the samples. For all three MNP treatments, the relative abundance of *S. wadsworthensis* appeared to be significantly lower in comparison with the control samples. The least concentrated NP treatments had a major impact on the number of sequences detected. The

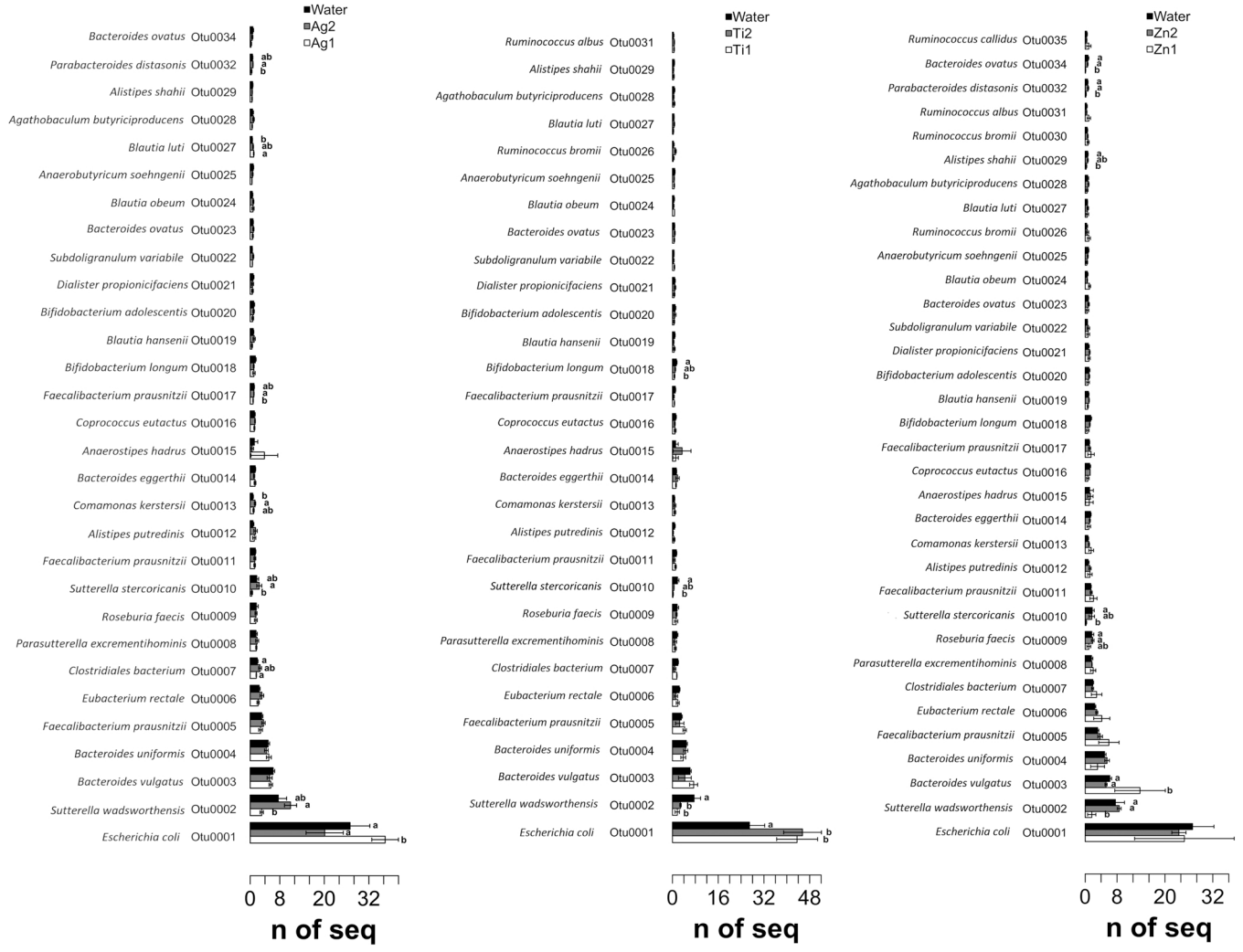

Fig. 2. Metastats model to assess the effect of the samples on the relative abundances of OTUs comprising 95% of the bacterial diversity divided by the three nanoparticle aqueous samples, from the left: Ag, Ti and Zn. Bars indicate the relative abundance of each OTU for control, low concentrated (labeled with number 1) and high concentrated (labeled with number 2). OTUs showing significant differences between treatments, according to the false discovery rate correction are highlighted with letters.

relative abundance of *Sutterella stercoricanis* decreased following Ag and TiO_2 NPs treatments (Fig. 2). Moreover, MNPs presence was correlated to the modulation of other genera such as *Bacteroides*, *Roseburia, Bifidobacterium, Fecalibacterium*, *Blautia* and *Alisteps*. As shown in Fig. 2, both Ag treatments increased *Blautia luti*, while *Bacteroides vulgatus* relative abundance was significantly high for the low-concentration ZnO treatment. Both concentrations of TiO_2 significantly reduced the relative abundance of *Bifidobacterium longum*.

Fig. 3 shows the results for the bacterial α-diversity of samples. The plot shows that two treatments promoted a statistically significant decrease in bacterial diversity compared to the control: the higher TiO_2 concentration (Ti_dioxide_Conc1) and the lower ZnO concentration (Zn_oxide_Conc2). The treatments Ag MNPs Conc1 and TiO_2 concentration 1 promoted a low diversity, despite being non-statistically different from the control. PICRUSt2 pathway prediction revealed significant differences between controls and specific treatments. Significantly modulated pathways were plotted as heat map and bar plots and are included in the supplementary materials (images Sup.1 and Sup.2). The major effect measured on specific pathways was due to Ag and TiO_2 at low concentration and TiO_2 at a high concentration. In Ag at low concentrations, significant pathways were linked to an increased abundance of *E.coli*. In addition, phenolic compound degradation (HCAMHPDEG-PWY, PWY-6690), *E.coli* lipid biosynthesis (KDO-NAGLIPASYN-PWY), and threonine degradation (THREOCAT-PWY) were found to be positively modulated by the treatment. TiO_2 in low concentrations caused a broad modulation of several pathways, including a specific pathway for menaquinones synthesis (PWY-6263) that could be linked to an increased abundance of *E.coli*. Moreover, TiO_2 predicted pathways resulted in several modulations related to arginine degradation (AST-PWY), enterobacterial common antigens (ECASYN-PWY) and ppGpp biosynthesis (PPGPPMET-PWY).

3.2. Metabolomic analysis

The untargeted metabolomics profiling of *in-vitro* digested water samples spiked with MNPs allowed the detection of 689 MS/MS metabolites (supplementary Table S1). The effect of MNPs on gut metabolome was first naively evaluated by an unsupervised multivariate HCA, as shown in Fig. 4. The HCA revealed MNPs had a significant effect on gut metabolic profiling, depending on their concentrations. Two different clusters were generated by the HCA, showing a clear metabolome similarity between Ag and ZnO at high concentrations and the control samples (first cluster), whereas all the lowest levels of MNPs exhibited a differentiated profile (second cluster). The main differences reported in HCA were investigated through fold change analysis obtained through a pairwise comparison between the MNPs treated and control samples (Supplementary Table S2). The gut metabolism after MNPs treatments showed a robust modulation of several compounds that were mainly related to the metabolisms of proteins, fatty acids, and polysaccharides. Furthermore, a general up-modulation of cholic and bile acids and a down-modulation of uric acids were reported in the gut environment after MNPs exposure. As indicated in Supplementary Table S2, the treatments with low concentrations of ZnO and Ag NPs produced an up-modulation of protein-driven metabolites, such as peptides and free amino acids. Among these protein-driven metabolites, the detection of metabolites derived from the catabolism of basic and aromatic amino acids, such as compounds containing indole, polyamines, and histamines, has attracted greater attention. Fatty acids metabolism was also affected by MNPs treatments. Both concentrations of TiO_2 NPs caused a general down-accumulation of fatty acids compared to Ag and ZnO NPs. However, in all treatments a highly up modulation of leukotriene B4 and prostaglandins was reported (Supplementary Table S2).

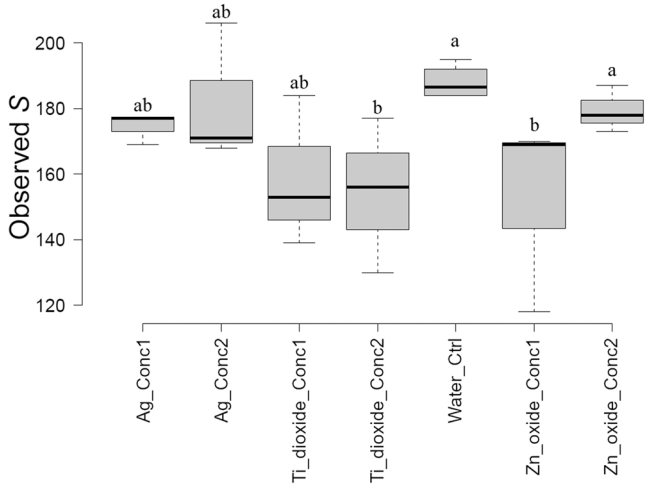

Fig. 3. Biodiversity of bacteria, as affected by the different MNPs treatments and concentrations, according to Sobs index, the presence of letters indicates a statistical significance of $p \leq 0.05$ for LSD test.

Given the distinctive metabolic profile of the two MNPs concentration levels, an additional supervised multivariate orthogonal projection to latent structures discriminant analysis (OPLS-DA) was carried out to clearly understand the differences among MNPs on gut microbiota at low and high (Fig. 5) concentrations. The OPLS-DA model was characterized by high robustness in goodness-of-fit and the ability to make a prediction. For the OPLS-DA model, a list of variable importance in projection (VIP) discriminant markers was extrapolated to provide insight into the metabolic markers mostly involved in such discrimination (Supplementary Table S3).

The OPLS-DA model revealed a clear gut metabolomic effect due to the different treatments. Among different MNPs, Ag and ZnO NPs in high concentrations showed a more differentiated profile when compared with the other treatments. The OPLS-DA model was in accordance with the HCA outcome, with prostaglandins and cholic and bile acids, as well as short-chain fatty acids, which were identified as most discriminant and up accumulated in the presence of high levels of ZnO and TiO_2 NPs. In contrast, xanthines and long and medium-chain fatty acids were harshly repressed (Supplementary Table S2). At low concentrations, all the treatments as well as TiO_2 in high concentration showed a similar profile, based on HCA, with bile acids, amines, and indole-containing compounds accumulated in the presence of low Ag and ZnO NPs peptides and down-accumulated derivatives (Supplementary Table S2).

3.3. Chemical similarity enrichment analysis

The metabolomics analysis was interpreted by using a statistical enrichment approach based on chemical similarity: the compounds were differentially modulated by MNP treatments and compared to the control (Fig. 6). Overall, the effect of highly concentrated MNPs on the gut microbiota was less evident than that of MNPs with a low concentration. Regarding Ag NPs (Fig. 6A, B), a low Ag level caused a deeper metabolic effect, which promoted an accumulation of cholic acids and butanols, whereas indoles and xanthines were mostly down-accumulated. ZnO NPs promoted a slight metabolic effect on the gut microbiota, which was probably due to the role of Zn as an important mediator of gut microbiota integrity and diversity (Fig. 6C, D). The lowest level of TiO_2 NPs had a diversified metabolic effect on the gut microbiota; in particular, it caused an accumulation of unsaturated fatty acids and acetophenones, and it played a negative role in the accumulation of carotenoids, peptides and benzopyrans.

3.4. Integration data

The omics data integration method is based on generalized partial least squares discriminant analysis (PLS-DA) for multiple datasets, and it

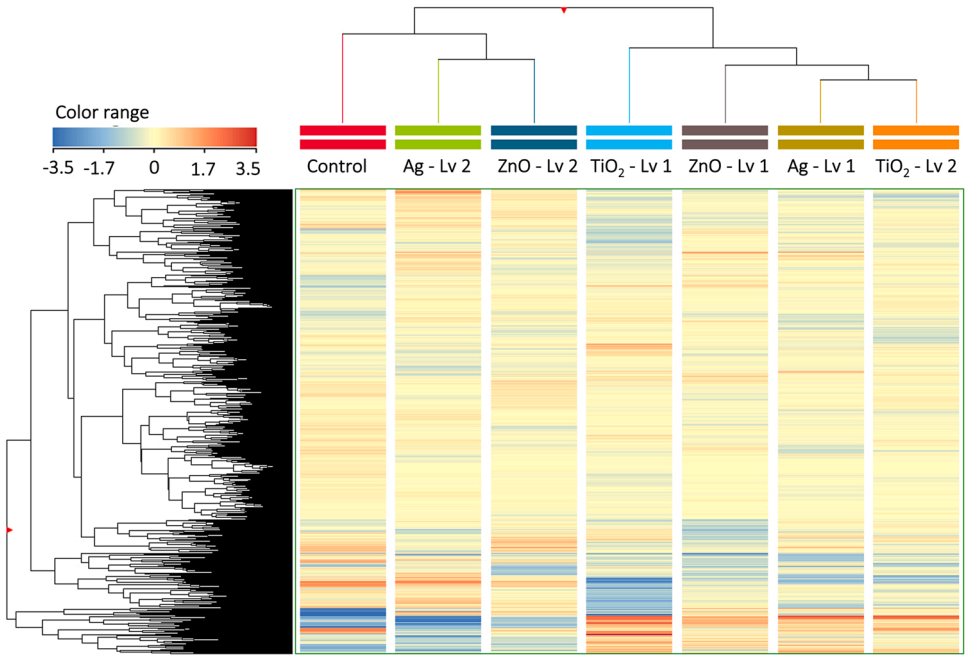

Fig. 4. Unsupervised hierarchical cluster analysis of gut metabolites after treatment with higher and lower concentrations of Ag, TiO_2, and ZnO nanoparticles. The fold change values for each compound were calculated with respect to the median of all samples and further used to obtain a fold change-based heatmap according to Ward's linkage algorithm (Euclidean distance).

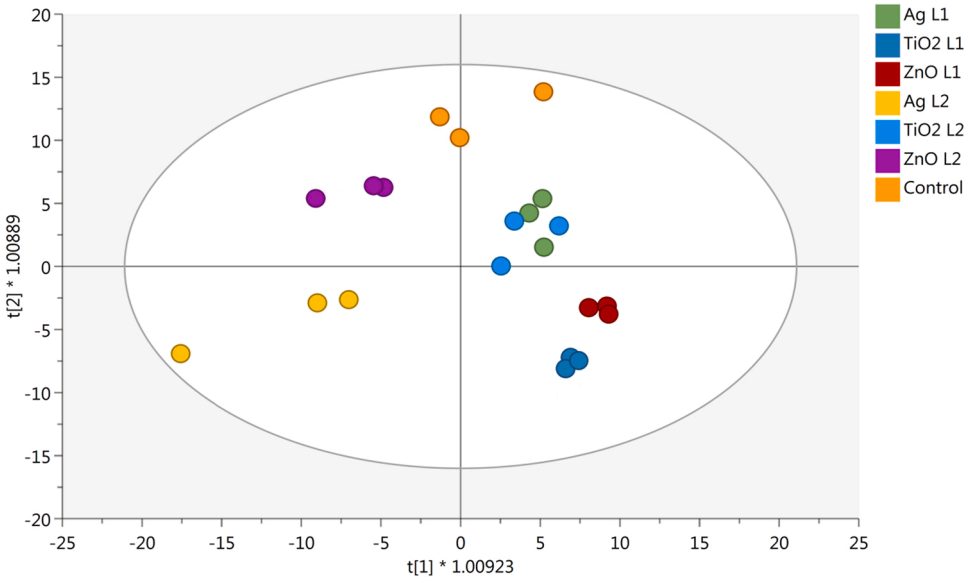

Fig. 5. Orthogonal projection to latent structures discriminant analysis (OPLS-DA) of gut metabolites after treatment with lower and higher concentrations of Ag, TiO_2, and ZnO nanoparticles.

is correlated with the sparce Generalized Canonical Correlation Analysis (sGCCA) method used for maximizing the covariance between linear combinations of variables (latent component scores) and projecting the data into the smallest dimensional subspace spanned by the components. The metabolomics and sequencing datasets were checked individually to evaluate their distribution. The 2 PLS-DA models reported 38% and 42% of discrimination capacity for the first 2 components, as sequencing and metabolomics datasets, respectively.

The integration of both datasets was shown as a heat map that considered the most discriminating compounds belonging to the first three components (Fig. 7A) of the PLS-DA model. Apart from TiO_2, all MNPs with a low concentration caused a more evident effect than did the control samples. In Fig. 7A, the heat map of most discriminant features revealed two separate clusters: the first cluster was composed of controls and samples with high concentration of Ag and ZnO. The second comprised Ag and ZnO at low concentrations and TiO_2 at high concentrations. As shown in the figure, a clear similarity in regulation was observed for the omics variables belonging to the two datasets. Moreover, their correlation trend was confirmed through Pearson's correlation analysis of selected variables for each component (Fig. 7B). Specifically, the first 3 principal components were characterized by significant positive correlation coefficients: $r = 0.84$, $r = 0.77$, and $r = 0.77$, respectively, thus indicating a satisfactory discriminatory potential of the selected variables among treatments.

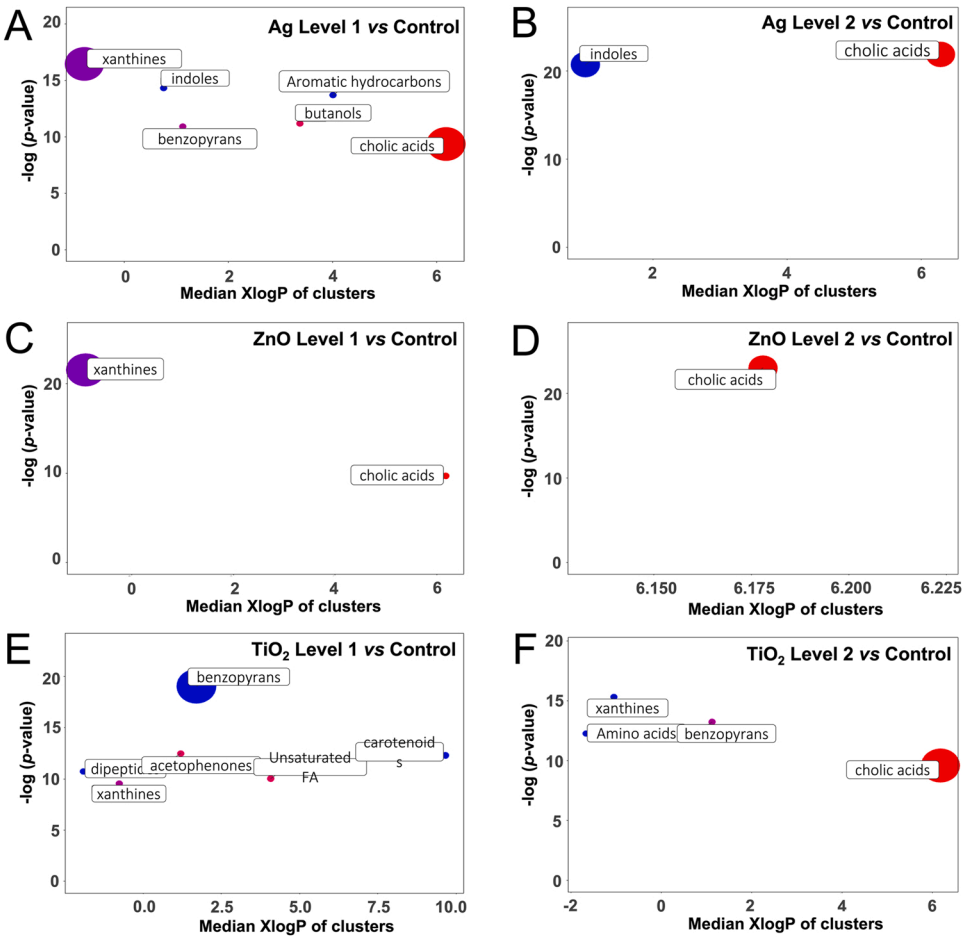

Fig. 6. ChemRICH set enrichment statistics plot. Each node reflects a significantly altered cluster of metabolites. Enrichment p-values are given by ANOVA test. Node sizes represent the total number of metabolites in each cluster set. The node color scale shows the proportion of increased (red) or decreased (blue) compounds detected in gut metabolome treated with respectively higher and lower concentrations of (A) and (B) AgNPs; (C) and (D) ZnO NPs; (E) and (F) TiO_2 NPs. Purple-color nodes have both increased and decreased metabolites.

Finally, the most discriminant and correlated features between multi-omics datasets were selected for the first three principal components (Fig. 7C, D, E). The list of the most relevant OTUs and metabolites is reported in Supplementary Table S4. The first and second components were found to have great discriminatory potential, as they explained ~ 40% of total differences and possessed higher discriminative power between the effect of TiO_2 NPs on gut metabolism than those of ZnO and Ag NPs. The model positively correlated *E. coli*, *S. wadsworthensis*, and *B. vulgatus* to 9,10-epoxyoctadecenoic acid and acetylspermidine in samples treated with TiO_2 NPs at a low concentration. Furthermore, several dipeptides, polyamines, and prostaglandins correlated to *Clostridium thermocellum, Clostridium populeti, E.coli,* and *Parabacteroides distasonis* in samples treated with ZnO and Ag NPs at low concentrations.

A high TiO_2 NPs concentration resulted in behavior similar to that of a high ZnO NPs concentration, which was characterized by the correlation between *B. vulgatus, Bacteroides uniformis, Bacteroides caccae, Bacteroides eggerthii*, *E. coli,* and *S. wadsworthensis* with dipeptides and the amino acid lysine.

4. Discussions

MNPs are often employed as food additives due to their coloring and opacifying properties that are used to improve the appearance and taste of processed foods. Exposure to MNPs occurs principally through oral intake, inhalation, and dermal contact. Recent studies have confirmed that MNPs can easily cross the gut barrier and affect gut homeostasis and spread to other organs, causing an immunological response [29]. For these reasons, the metabolomic effect of three MNPs, namely ZnO, TiO_2, and Ag, at two different concentrations were examined after *in-vitro* digestion to simulate their effects during the digestive process. The *in-vitro* digestion of MNPs was carried out using salivary, gastric, and intestinal fluids, and subsequent fecal fermentation. After the fermentation, all samples were examined using an integrated multi-omics approach (sequencing and metabolomics) to shed light on their effects on gut microbiota and the large intestine fermentation process. The sequencing analysis showed that the most significant effects of MNPs on OTU abundances and diversity were observed in the least rather than the most concentrated samples. Hierarchical clustering analyses (HCA) at the family level showed an overall predominance of *Enterobacteriaceae, Bacteroidaceae, Lachnospiraceae,* and *Ruminococcaceae* (Fig. 1), families commonly found within the human gut. Great differences between groups were not found, suggesting a modulation of species within family groups rather than a shift in microbial families. However, both low and high concentrations showed a clear increase in *Enterobacteriaceae* in TiO_2-treated samples. Furthermore, when looking at specific species, 16 S amplicon sequencing analysis revealed a clear modulation mediated by the addition of MNPs. For Ag and TiO_2 treatments, especially in low concentrations, a significant increase in *E. coli* abundance was found. This result is consistent with the findings from PICRUSt2, which highlighted several pathways such as phenolic compound degradation (HCAMHPDEG-PWY, PWY-6690), lipid biosynthesis (KDO-NAGLIPA-SYN-PWY), and threonine degradation (THREOCAT-PWY) that are related to *E. coli* metabolism. An enrichment in the *E. coli* population does not directly result in impaired intestinal functionality, because in healthy individuals the *E. coli* gut population is mostly represented by commensal strains. However, an increased relative abundance of *E. coli* within the gut is usually associated with different pathologies and has been identified in IBD patients [40]. Moreover, a general increase in *E. coli* in IBD cases is associated with the development of pathogenic adherent strains and a decline in commensal and positive bacterial

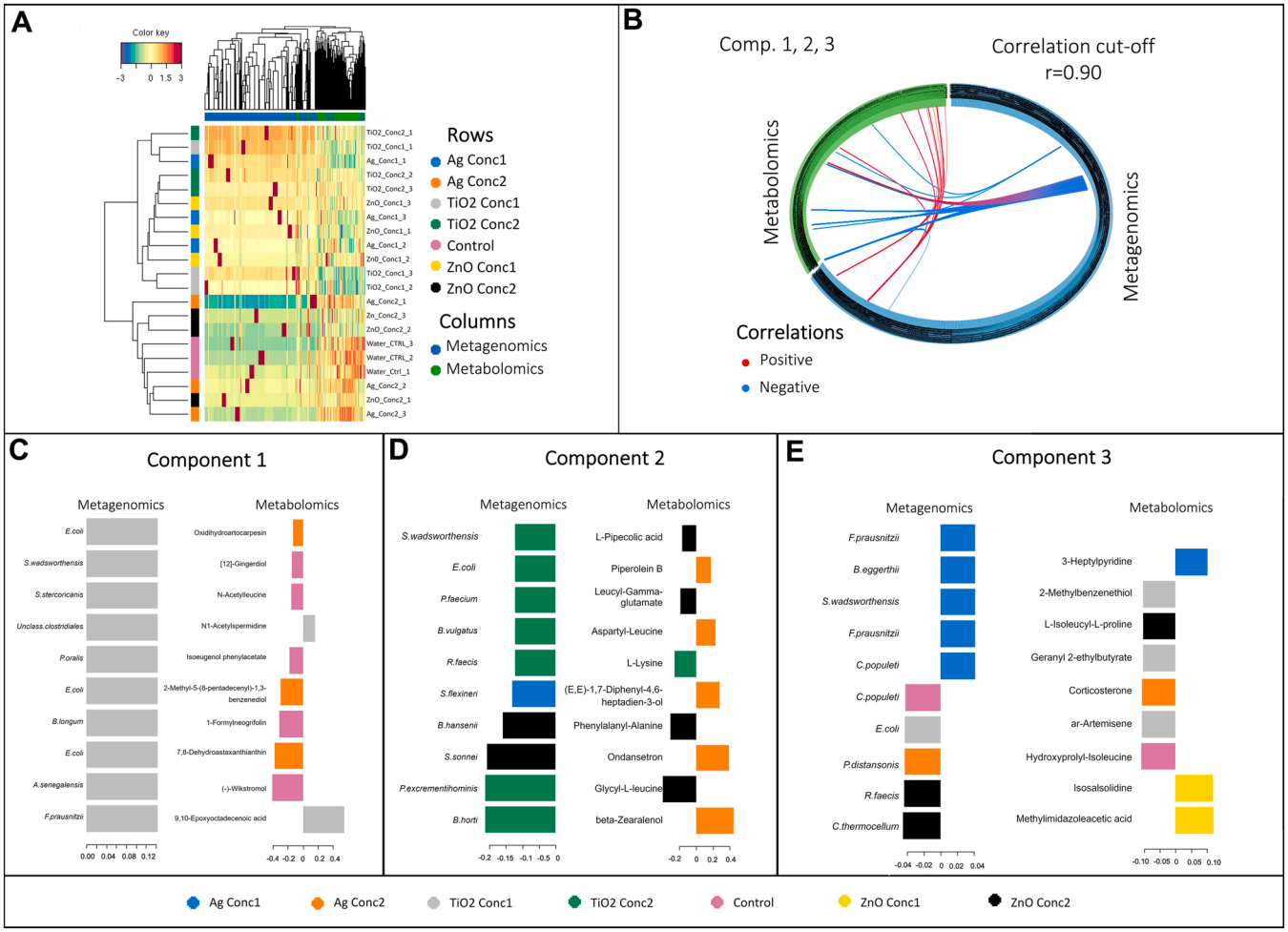

Fig. 7. (A) Heatmap correlation plot of most discriminant features selected in metabolomics and metagenomics datasets. Samples are represented in rows, selected features on the first three principal components of the sPLS-DA in columns. (B) Circos plot was carried out using Pearson correlation coefficients ($r > 0.9$). The plot shows the positive (red) and negative (blue) correlation between the selected features of the two datasets. (C-E) Loading plot of each feature selected having the maximal discrimination ability on the first (C), second (D) and third (E) component in each omics datasets, with color indicating the class with a maximal mean discriminant value.

species which provide a protective layer on a host's intestine [46]. An increased *E. coli* relative abundance has also been found in patients with Crohn's disease and is linked with the development of different strains, possessing pathogenic traits, such as the production of invasins and adhesins [46]. The relative abundance of *B. vulgatus* was increased by the lowest concentration of ZnO. Interestingly, a multi-omic study has recently associated the ulcerative colitis (UC) disease in humans with the accumulation of *B. vulgatus*, thus highlighting the microorganism's responsibility for approximately 50% of microbial proteins involved in UC [44]. The genus *Sutterella* was significantly reduced in all the treatments; in particular, *S. wadsworthensis* was reduced by low MNP concentrations. This latter species is considered a gut commensal bacterium that primarily colonizes the mucus layer in the small intestine tract [31]. The effects of *Sutterella sp.* on the human gut are still debated; some authors have reported a high abundance of the genus in healthy prebiotic-treated mice [20], whereas others link an accumulation of *Sutterella* with autism spectrum disorders [18]. Significant modulation due to MNPs of TiO_2 at a low concentration was also observed with *Bifidobacterium longum*, a well-known multifunctional probiotic that is effective in alleviating gastrointestinal, immunological, and infectious diseases while stabilizing the gut microbiota [69]. One of the effects of *B. longum* reduction could be a susceptibility of the host to the adhesion of pathogens to the intestinal surface as well as a general impact on intestinal homeostasis.

The treatment with different MNPs on the gut metabolome caused a marked impairment in the metabolism of different chemical classes, that are mainly related to protein metabolism. These chemical classes include xanthine, polyamines, indole derivatives, peptides, and other metabolites in the large intestine. The presence of proteins is usually derived from the diet: there is a direct correlation between the amount of dietary-ingested protein and the protein content that reaches the large intestine and becomes ready for proteolytic fermentation [36,68]. Moreover, even in small quantities, material that reaches the large intestine has traces of sloughed cells, pancreatic enzymes, and bile acids that may flow past the ileum [16]. The fermentation of protein is usually associated with the action of bacterial proteases that generate a broad diversity of metabolites, including peptides, free amino acids, amines, keto-acids, branched fatty acids, phenols and indoles that accumulate in the colon [12]. Present findings showed a down-accumulation of several peptides in samples treated with low concentrations of MNPs, compared to the controls. This could be related to the enrichment of bacterial species with high proteolytic activity, namely *B. vulgatus* and *E. coli*, which were significantly abundant in the treated samples. As is well known, an altered host microbiota homeostasis and function are usually associated with inflammatory bowel diseases (IBD) or irritable bowel syndrome (IBS) diseases, including UC. Recent studies reported a differential microbiota composition in UC patients compared to healthy individuals; in particular, metagenomics analysis of fecal samples

identified a large number of proteases/peptidases elastases-related genes in UC patients [22,32]. Particularly, the delivery of ZnO NPs at low concentrations resulted in a significant enrichment of *B. vulgatus* and a significant overall down-accumulation of peptides. This result was consistent with what was reported by Mills et al. [44], who observed an overabundance of proteases originating from *B. vulgatus* in clinically active UC patients. Surprisingly, the omics data integration analysis highlighted a correlation between the enrichment of dipeptides and *B. vulgatus*, *Clostridium* spp., and *E. coli*. Accordingly, significant modulation of the relative abundance of *E. coli* was also observed in treatments with a low concentration of Ag and TiO_2 NPs. *Bacteroides* are among the amplest genus present in the gut; they are located in the outer mucosal layer of the colon and some researchers indicate they are responsible for ~27% of proteolytic activity in UC patients [33,43].

High proteolytic activity of proteins/peptides often releases free amino acids. However, ZnO NPs in low concentration and TiO_2 NPs in both high and low concentrations caused the lowest free amino acids content of all treatments, thus suggesting a higher uptake and metabolic activity of free amino acids by bacteria. Peptides or free amino acids are usually transported into the microbial cell and transformed into several metabolites, including biogenic amines, phenol, and indole, which exert effects on the barrier integrity of the gut mucosa [64]. This result is consistent with PICRUSt2 findings which highlighted a significant increase in protein degradation pathways, especially L-arginine degradation (AST-PWY). Accordingly, we detected an up-accumulation of N1-acetylspermidine and N5-hexanoylspermidine in MNP-treated samples, resulting from the decarboxylation of basic amino acids [48]. Integration analysis revealed that the enrichment of the N-acetylspermidine metabolite is also correlated to the abundance of *E. coli* in low-concentration TiO_2 samples; this metabolite has previously been linked to shock response in *E. coli*, thus highlighting a treatment-induced stress condition [14]. Moreover, aromatic amino acids fermentation products such as indole-3-acetic acid, indole-3-carboxaldehyde, and indole-3-propanoic acid were also modulated. These compounds are said to be crucial in the severity of IBS and IBD pathology. Indole-3-propionic acid has been shown to be down-modulated in UC patients [2]. Our results show a clear correlation between the effects of specific nanometals and the modulation of bacterial species and metabolites. For Ag NPs, especially at low concentrations, the most modulated microorganisms we identified were *E. coli, S. wadsworthensis, B. luti*, and *P. distansonis*. Treatment with Ag NPs caused an overall down-accumulation of indoles and their derivatives, and the resulting perturbation has a great influence on gastrointestinal disorders and is also regarded as negatively altered in IBD patients [38].

In addition, in TiO_2 NPs (either at low or high concentrations) and ZnO NPs (at high concentrations) treated samples, a down-accumulation of indole-3-acetic acid was reported. This metabolite was found to be decreased after antibiotic administration in rats [7], and this administration led to an increase in the susceptibility of the rats to chronic inflammatory diseases such as IBS [37]. Indole-3-acetic acid is a ligand of the aryl hydrocarbon receptor (AhR), which is an important transcription factor that is widely expressed in immune and non-immune gut cells and is highly correlated to inflammatory processes, including the outcome of IBD [34,35,60]. We detected an enrichment of arachidonic acid metabolites, such as prostaglandin E2 and leukotrienes B4. This detection highlights the inflammatory process induced by MNP application in gut microbiota. This inflammatory process is particularly driven by TiO_2 NP treatment. The arachidonic acid metabolites are pro-inflammatory lipid mediators that are found to be highly expressed in the early stage of the inflammatory process [61,62]. Moreover, omics data integration correlated the modulation of *S. wadsworthensis* and *E. coli* to the 9,10-epoxyoctadecenoic acid compounds in samples with a low concentration of TiO_2, which represent an autoxidation product of linolenic acid and is involved in the regulation of the inflammation process associated with liver disease [3].

Our results showed that lower MNPs concentrations had a greater impact than the higher concentrations, which corroborates the thesis about the aggregation behavior of MNPs. This phenomenon is mostly affected by pH and electrolyte concentration as well as by the presence of biomolecules that can affect MNPs stability and toxicity [9,63]. Aggregation effects can limit adverse effects on living cells (Bélteky et al., 2019). The authors demonstrated that a high aggregation grade of Ag NPs samples attenuated the toxic effects on living cells by reducing the biological activity of the cells. Low concentrations of Ag and ZnO resulted in heightened effects, whereas TiO_2 NPs showed toxicity even at higher concentrations. This could be explained by the interaction of MNPs with their immediate environment and with colloidal stability factors. For instance, Ag NPs have often been observed to be modified by gastric fluids, due to the acidic environment. The latter contains a high Cl^- concentration that can dissolve Ag NPs to generate precipitation of AgCl [4]. Conversely, the chemical properties of TiO_2 NPs provide the possibility for many biomolecules to be adsorbed, thus modifying their reactivity and interaction with their immediate environment [47]. Bianchi et al. [11] showed the synergistic effect of lipopolysaccharides adsorbed by TiO_2 NPs, resulting in the potentiation of pro-inflammatory effects [11].

The present work presents some strengths and limitations worth highlighting. Firstly, this is one of the first studies that has applied an integrated omic-based approach to investigate the role of different NPs that are relevant to human nutrition and health and human gut microbiota modulation. Secondly, the concentrations used in this model were consistent with typical dietary intake, thus mimicking a potentially real *in-vivo* situation. The *in vitro* gastrointestinal digestion model used was applied before fecal fermentation to expose NPs to modifications possibly occurring *in-vivo* before investigating the effect on the gut microbiome and metabolome. The *in-vitro* digestion and fecal fermentation model presents some limitations. The non-dynamic and varying steps of digestion and fermentation applied are not close to the real condition which may occur *in-vivo*. However, due to the small volumes of analysis, we adopted a digestion model which accurately simulates the gastrointestinal tract. Moreover, we did not consider the estimated *in-vitro* bioavailability, which may represent a relevant *in-vivo* physiological step. This physiological mechanism should be better investigated for NPs by using other *in-vitro* models that have not been considered in the present work. Concerning the latter, it is important to highlight that the aim of the present work was not to specifically determine the rate of absorption *in-vitro*, but rather to evaluate the potential effect of NPs that are not absorbed in the first GIT on gut microbiota and metabolites produced during fermentation. These NPs were incubated with fecal slurry after undergoing modifications that may potentially occur during the first oral–gastric–small intestine steps.

5. Conclusions

In the present work, multiple omics were used to assess the effects of three different metal NPs (TiO_2, ZnO, and Ag) at different concentrations on the gut microbiome and metabolome following *in-vitro* digestion and fecal fermentation. The different metal NPs showed a reduction in α-diversity especially for ZnO MNPs at low concentration, and TiO_2 NPs at high concentrations. Ag and TiO_2 MNPs in low concentrations caused an increased relative abundance of *E. coli*, which is usually associated with bowel irritation, while low concentration of ZnO NPs resulted in a significant enrichment of *B. vulgatus* and a substantial down-accumulation of overall peptides whose activity is linked to the activity of proteolytic bacteria species. Accordingly, omics data integration analysis highlighted a positive correlation between the presence of dipeptides and the enrichment of *Bacteroides spp*., as well as *E. coli*, suggesting the production of proteases by this species. Using PICRUSt2 analysis, we also found that pathways related to proteolysis are positively modulated in both Ag- and TiO_2- treated samples. Moreover, low concentrations of TiO_2 caused a reduction in *B. longum*, a well-known probiotic bacterium that is important for gut health and functionality.

The treatment with different MNPs caused a significant difference from the control, and a broad diversity of metabolites were modulated, including xanthine, polyamines, indole derivatives, peptides, and metabolites related to protein metabolism in the large intestine. The results of this research corroborate the theory of in-gut aggregation of MNPs, thus showing low concentrations of Ag and ZnO MNPs have a more pronounced impact on the gut microbiome and metabolome compared to high concentrations. An interesting note must be made for TiO_2 which at high concentrations did not reduce the alteration of the microbiome and metabolome and instead caused an intensification of effects. The chemical properties of TiO_2 NPs offer the possibility of adsorption to increased sizes without changing the toxic characteristics of the NPs. It is known that particle aggregation is modulated by multiple factors such as pH, electrolyte concentration, and biomolecules that can affect MNP stability and toxicity. Notwithstanding, we do not fully know the consequences of this aggregation on NP biological effects. In the future, this aggregation should receive research attention to clearly define its causes and effects on intestinal homeostasis and human health.

CRediT authorship contribution statement

Filippo Vaccari: Conceptualization, Methodology, Formal analysis, Writing – original draft. **Leilei Zhang**: Conceptualization, Methodology, Formal analysis, Writing – original draft. **Alfina Grasso**: Methodology, Formal analysis, Writing – review & editing. **Francesca Bandini**: Writing – review & editing. **Pascual García-Pérez**: Formal analysis, Writing – review & editing. **Chiara Copat**: Conceptualization, Formal analysis, Writing. **Luigi Lucini**: Conceptualization, Writing – review & editing, Supervision. **Margherita Dall'Asta**: Conceptualization, Writing – review & editing, Supervision. **Margherita Ferrante**: Conceptualization, Writing – review & editing, Supervision. **Edoardo Puglisi**: Conceptualization, Software, Writing – review & editing, Supervision. **Gianluca Giuberti**: Conceptualization, Formal analysis, Writing – review & editing, Supervision.

Declaration of Competing Interest

The authors declare that they have no known competing financial interests or personal relationships that could have appeared to influence the work reported in this paper.

Data availability

Data will be made available on request.

Acknowledgments

Part of this research was supported by the project "Impacts of environmental risk factors on oncologic, cardiorespiratory and neurodegenerative diseases", financed by Università Cattolica del Sacro Cuore within the D3.2 2021 funding scheme.

PGP acknowledges the "Margarita Salas" grant supported by the European Union through the "NextGenerationEU" program from the University of Vigo.

Appendix A. Supplementary material

Supplementary data associated with this article can be found in the online version at doi:10.1016/j.jhazmat.2023.131331.

References

[1] Adeyeye, S.A.O., Ashaolu, T.J., 2021. Applications of nano-materials in food packaging: a review. J Food Process Eng 44 (7). https://doi.org/10.1111/jfpe.13708.

[2] Alexeev, E.E., Lanis, J.M., Kao, D.J., Campbell, E.L., Kelly, C.J., Battista, K.D., et al., 2018. Microbiota-derived indole metabolites promote human and murine intestinal homeostasis through regulation of interleukin-10 receptor. Am J Pathol 188 (5), 1183–1194. https://doi.org/10.1016/j.ajpath.2018.01.011.

[3] Anton, P., Rutt, L.N., Capper, C., McCullough, R., 2022. Profiling the oxylipidome in aged mice after chronic ethanol feeding: identifying a disconnect between cytokines and lipid metabolites. SSRN Electron J. https://doi.org/10.2139/ssrn.4093290.

[4] Axson, J.L., Stark, D.I., Bondy, A.L., Capracotta, S.S., Maynard, A.D., Philbert, M. A., et al., 2015. Rapid kinetics of size and pH-dependent dissolution and aggregation of silver nanoparticles in simulated gastric fluid. J Phys Chem C 119 (35), 20632–20641. https://doi.org/10.1021/acs.jpcc.5b03634.

[5] Bartram, A.K., Lynch, M.D.J., Stearns, J.C., Moreno-Hagelsieb, G., Neufeld, J.D., 2011. Generation of multimillion-sequence 16S rRNA gene libraries from complex microbial communities by assembling paired-end illumina reads. Appl Environ Microbiol 77 (11), 3846–3852. https://doi.org/10.1128/AEM.02772-10.

[6] Barupal, D.K., Fiehn, O., 2017. Chemical similarity enrichment analysis (ChemRICH) as alternative to biochemical pathway mapping for metabolomic datasets. Sci Rep 7 (1), 1–11. https://doi.org/10.1038/s41598-017-15231-w.

[7] Behr, C., Ramírez-Hincapié, S., Cameron, H.J., Strauss, V., Walk, T., Herold, M., et al., 2018. Impact of lincosamides antibiotics on the composition of the rat gut microbiota and the metabolite profile of plasma and feces. Toxicol Lett 296 (August), 139–151. https://doi.org/10.1016/j.toxlet.2018.08.002.

[8] Bellmann, S., Carlander, D., Fasano, A., Momcilovic, D., Scimeca, J.A., Waldman, W.J., et al., 2015. Mammalian gastrointestinal tract parameters modulating the integrity, surface properties, and absorption of food-relevant nanomaterials. Wiley Interdiscip Rev Nanomed Nanobiotechnol 7 (5), 609–622. https://doi.org/10.1002/wnan.1333.

[9] Bergin, I.L., Witzmann, F.A., 2013. Nanoparticle toxicity by the gastrointestinal route: evidence and knowledge gaps. Int J Biomed Nanosci Nanotechnol 3 (1–2). https://doi.org/10.1504/IJBNN.2013.054515.

[10] Berry, D., Mahfoudh, K., ben, Wagner, M., Loy, A., 2011. Barcoded primers used in multiplex amplicon pyrosequencing bias amplification. Appl Environ Microbiol 77 (21), 7846–7849. https://doi.org/10.1128/AEM.05220-11.

[11] Bianchi, M.G., Allegri, M., Chiu, M., Costa, A.L., Blosi, M., Ortelli, S., et al., 2017. Lipopolysaccharide adsorbed to the bio-corona of TiO2 nanoparticles powerfully activates selected pro-inflammatory transduction pathways. Front Immunol 8 (August). https://doi.org/10.3389/fimmu.2017.00866.

[12] Blachier, F., Mariotti, F., Huneau, J.F., Tomé, D., 2007. Effects of amino acid-derived luminal metabolites on the colonic epithelium and physiopathological consequences. Amino Acids 33 (4), 547–562. https://doi.org/10.1007/s00726-006-0477-9.

[13] Bortolini, C., Patrone, V., Puglisi, E., Morelli, L., 2016. Detailed analyses of the bacterial populations in processed cocoa beans of different geographic origin, subject to varied fermentation conditions. Int J Food Microbiol 236, 98–106. https://doi.org/10.1016/j.ijfoodmicro.2016.07.004.

[14] Carper, S.W., Willis, D.G., Manning, K.A., Gernerg, E.W., 1991. Spermidine acetylation in response to a variety of stresses in Escherichia coli. J Biol Chem 19, 12439–12441. https://doi.org/10.1016/S0021-9258(18)98917-9.

[15] Caspi, R., Altman, T., Billington, R., Dreher, K., Foerster, H., Fulcher, C.A., et al., 2014. The MetaCyc database of metabolic pathways and enzymes and the BioCyc collection of pathway. Genome Databases 42 (November 2013), 459–471. https://doi.org/10.1093/nar/gkt1103.

[16] Chacko, A., Cummings, J.H., 1988. Nitrogen losses from the human small bowel: obligatory losses and the effect of physical form of food. Gut 29 (6), 809–815. https://doi.org/10.1136/gut.29.6.809.

[17] de Vos, S., Waegeneers, N., Verleysen, E., Smeets, K., Mast, J., 2020. Physico-chemical characterisation of the fraction of silver (nano)particles in pristine food additive E174 and in E174-containing confectionery. Food Addit Contam Part A Chem Anal Control Expo Risk Assess 37 (11), 1831–1846. https://doi.org/10.1080/19440049.2020.1809719.

[18] Ding, H.T., Taur, Y., Walkup, J.T., 2017. Gut microbiota and autism: key concepts and findings. J Autism Dev Disord 47 (2), 480–489. https://doi.org/10.1007/s10803-016-2960-9.

[19] Dixon, P., 2003. VEGAN, a package of R functions for community ecology. J Veg Sci 14 (6), 927–930. https://doi.org/10.1111/j.1654-1103.2003.tb02228.x.

[20] Everard, A., Lazarevic, V., Gaïa, N., Johansson, M., Ståhlman, M., Backhed, F., et al., 2014. Microbiome of prebiotic-treated mice reveals novel targets involved in host response during obesity. ISME J 8 (10), 2116–2130. https://doi.org/10.1038/ismej.2014.45.

[21] Fontana, A., Patrone, V., Puglisi, E., Morelli, L., Bassi, D., Garuti, M., et al., 2016. Effects of geographic area, feedstock, temperature, and operating time on microbial communities of six full-scale biogas plants. Bioresour Technol 218, 980–990. https://doi.org/10.1016/j.biortech.2016.07.058.

[22] Galipeau, H.J., Caminero, A., Turpin, W., Bermudez-Brito, M., Santiago, A., Libertucci, J., et al., 2021. Novel fecal biomarkers that precede clinical diagnosis of ulcerative colitis. Gastroenterology 160 (5), 1532–1545. https://doi.org/10.1053/j.gastro.2020.12.004.

[23] Goñi-Ciaurriz, L., Vélaz, I., 2022. Antibacterial and degradable properties of β-cyclodextrin-TiO2 cellulose acetate and polylactic acid bionanocomposites for food packaging. Int J Biol Macromol 216, 347–360. https://doi.org/10.1016/j.ijbiomac.2022.06.202.

[24] Good, I.J., 1953. The population frequencies of species and the estimation of population parameters. Biometrika 40 (3/4), 237–264. ⟨http://www.jstor.org/stable/2333344⟩.

[25] Grasso, A., Ferrante, M., Arena, G., Salemi, R., Zuccarello, P., Fiore, M., et al., 2021. Chemical characterization and quantification of silver nanoparticles (Ag-nps) and dissolved ag in seafood by single particle icp-ms: assessment of dietary

exposure. Int J Environ Res Public Health 18 (8). https://doi.org/10.3390/ijerph18084076.
[26] Grasso, A., Ferrante, M., Moreda-Piñeiro, A., Arena, G., Magarini, R., Oliveri Conti, G., et al., 2022. Dietary exposure of zinc oxide nanoparticles (ZnO-NPs) from canned seafood by single particle ICP-MS: balancing of risks and benefits for human health. Ecotoxicol Environ Saf *231*. https://doi.org/10.1016/j.ecoenv.2022.113217.
[27] Grasso, A., Ferrante, M., Zuccarello, P., Filippini, T., Arena, G., Fiore, M., et al., 2020. Chemical characterization and quantification of titanium dioxide nanoparticles (Tio2-nps) in seafood by single-particle icp-ms: assessment of dietary exposure. Int J Environ Res Public Health 17 (24), 1–15. https://doi.org/10.3390/ijerph17249547.
[28] Halamoda-Kenzaoui, B., Ceridono, M., Urbán, P., Bogni, A., Ponti, J., Gioria, S., et al., 2017. The agglomeration state of nanoparticles can influence the mechanism of their cellular internalisation. J Nanobiotechnol 15 (1). https://doi.org/10.1186/s12951-017-0281-6.
[29] Heringa, M.B., Geraets, L., van Eijkeren, J.C.H., Vandebriel, R.J., de Jong, W.H., Oomen, A.G., 2016. Risk assessment of titanium dioxide nanoparticles via oral exposure, including toxicokinetic considerations. Nanotoxicology 10 (10), 1515–1525. https://doi.org/10.1080/17435390.2016.1238113.
[30] Herrera, G., Peña-Bahamonde, J., Paudel, S., Rodrigues, D.F., 2021. The role of nanomaterials and antibiotics in microbial resistance and environmental impact: an overview. Curr Opin Chem Eng *33*. https://doi.org/10.1016/j.coche.2021.100707.
[31] Hiippala, K., Kainulainen, V., Kalliomäki, M., Arkkila, P., Satokari, R., 2016. Mucosal prevalence and interactions with the epithelium indicate commensalism of Sutterella spp. Front Microbiol 7 (October), 1–13. https://doi.org/10.3389/fmicb.2016.01706.
[32] Hou, J.J., Wang, X., Li, Y., Su, S., Wang, Y.M., Wang, B.M., 2021. The relationship between gut microbiota and proteolytic activity in irritable bowel syndrome. Microb Pathog 157 (May), 104995. https://doi.org/10.1016/j.micpath.2021.104995.
[33] Hubbard, T.D., Murray, I.A., Bisson, W.H., Lahoti, T.S., Gowda, K., Amin, S.G., et al., 2015. Adaptation of the human aryl hydrocarbon receptor to sense microbiota-derived indoles. Sci Rep 5, 1–13. https://doi.org/10.1038/srep12689.
[34] Krishnan, S., Ding, Y., Saedi, N., Choi, M., Sridharan, G. v, Sherr, D.H., et al., 2018. Gut microbiota-derived tryptophan metabolites modulate inflammatory response in hepatocytes and macrophages. Cell Rep 23 (4), 1099–1111. https://doi.org/10.1016/j.celrep.2018.03.109.
[35] Lamas, B., Richard, M.L., Leducq, V., Pham, H.P., Michel, M.L., da Costa, G., et al., 2016. CARD9 impacts colitis by altering gut microbiota metabolism of tryptophan into aryl hydrocarbon receptor ligands. Nat Med 22 (6), 598–605. https://doi.org/10.1038/nm.4102.
[36] Landsiedel, R., Hahn, D., Ossig, R., Ritz, S., Sauer, L., Buesen, R., et al., 2022. Gut microbiome and plasma metabolome changes in rats after oral gavage of nanoparticles: sensitive indicators of possible adverse health effects. Part Fibre Toxicol 19 (1), 1–20. https://doi.org/10.1186/s12989-022-00459-w.
[37] Lavelle, A., Sokol, H., 2020. Gut microbiota-derived metabolites as key actors in inflammatory bowel disease. Nat Rev Gastroenterol Hepatol 17 (4), 223–237. https://doi.org/10.1038/s41575-019-0258-z.
[38] Li, X., Zhang, B., Hu, Y., Zhao, Y., 2021. New insights into gut-bacteria-derived indole and its derivatives in intestinal and liver diseases. Front Pharmacol 12 (December), 1–15. https://doi.org/10.3389/fphar.2021.769501.
[39] Marion-Letellier, R., Amamou, A., Savoye, G., Ghosh, S., 2019. Inflammatory bowel diseases and food additives: to add fuel on the flames. Nutrients 11 (5). https://doi.org/10.3390/nu11051111.
[40] Martinez-Medina, M., Garcia-Gil, L.J., 2014. Escherichia coli in chronic inflammatory bowel diseases: an update on adherent invasive Escherichia coli pathogenicity. World J Gastrointest Pathophysiol 5 (3), 213. https://doi.org/10.4291/wjgp.v5.i3.213.
[41] Martirosyan, A., Polet, M., Bazes, A., Sergent, T., Schneider, Y.-J., 2012. Food nanoparticles and intestinal inflammation: a real risk? In: Szabo, I. (Ed.), Inflammatory bowel disease. IntechOpen. https://doi.org/10.5772/52887.
[42] McDonald, D., Price, M.N., Goodrich, J., Nawrocki, E.P., DeSantis, T.Z., Probst, A., et al., 2012. An improved Greengenes taxonomy with explicit ranks for ecological and evolutionary analyses of bacteria and archaea. ISME J 6 (3), 610–618. https://doi.org/10.1038/ismej.2011.139.
[43] Mills, R., Dulai, P., Vázquez-Baeza, Y., Zhu, Q., Humphrey, G., DeRight Goldasich, L., et al., 2020. OP31 Meta–omics reveals microbiome-driven proteolysis as a contributing factor to the severity of ulcerative colitis disease activity. J Crohn's Colitis 14 (Suppl. 1), S030–S031. https://doi.org/10.1093/ecco-jcc/jjz203.030.
[44] Mills, R.H., Dulai, P.S., Vázquez-Baeza, Y., Sauceda, C., Daniel, N., Gerner, R.R., et al., 2022. Multi-omics analyses of the ulcerative colitis gut microbiome link Bacteroides vulgatus proteases with disease severity. Nat Microbiol 7 (2), 262–276. https://doi.org/10.1038/s41564-021-01050-3.
[45] Minekus, M., Alminger, M., Alvito, P., Ballance, S., Bohn, T., Bourlieu, C., et al., 2014. A standardised static in vitro digestion method suitable for food – an international consensus. Food Funct 5 (6), 1113–1124. https://doi.org/10.1039/C3FO60702J.
[46] Miquel, S., Peyretaillade, E., Claret, L., de Vallée, A., Dossat, C., Vacherie, B., et al., 2010. Complete genome sequence of crohn's disease-associated adherent-invasive E. coli strain LF82. PLoS ONE 5 (9), 1–16. https://doi.org/10.1371/journal.pone.0012714.
[47] Murugadoss, S., Brassinne, F., Sebaihi, N., Petry, J., Cokic, S.M., van Landuyt, K.L., et al., 2020. Agglomeration of titanium dioxide nanoparticles increases toxicological responses in vitro and in vivo. Part Fibre Toxicol 17 (1), 1–14. https://doi.org/10.1186/s12989-020-00341-7.
[48] Oliphant, K., Allen-Vercoe, E., 2019. Macronutrient metabolism by the human gut microbiome: major fermentation by-products and their impact on host health. Microbiome 7 (1), 1–15. https://doi.org/10.1186/s40168-019-0704-8.
[49] Olivares, M., Neef, A., Castillejo, G., de Palma, G., Varea, V., Capilla, A., et al., 2015. The HLA-DQ2 genotype selects for early intestinal microbiota composition in infants at high risk of developing coeliac disease. Gut 64 (3), 406–417. https://doi.org/10.1136/gutjnl-2014-306931.
[50] Paulson, J.N., Pop, M., Bravo, H.C., 2011. Metastats: an improved statistical method for analysis of metagenomic data. Genome Biol 12 (1), P17. https://doi.org/10.1186/gb-2011-12-s1-p17.
[51] Pérez-Burillo, S., Rufián-Henares, J.A., Pastoriza, S., 2018. Towards an improved global antioxidant response method (GAR+): physiological-resembling in vitro antioxidant capacity methods. Food Chem 239, 1263–1272. https://doi.org/10.1016/j.foodchem.2017.07.063.
[52] Puglisi, E., Romaniello, F., Galletti, S., Boccaleri, E., Frache, A., Cocconcelli, P.S., 2019. Selective bacterial colonization processes on polyethylene waste samples in an abandoned landfill site. Sci Rep 9 (1). https://doi.org/10.1038/s41598-019-50740-w.
[53] Rocchetti, G., Ghilardelli, F., Masoero, F., Gallo, A., 2021. Screening of regulated and emerging mycotoxins in bulk milk samples by high-resolution mass spectrometry. Foods 10 (9), 1–15. https://doi.org/10.3390/foods10092025.
[54] Rocchetti, G., Senizza, A., Gallo, A., Lucini, L., Giuberti, G., Patrone, V., 2019. In vitro large intestine fermentation of gluten-free rice cookies containing alfalfa seed (Medicago sativa L.) flour: a combined metagenomic/metabolomic approach. Food Res Int 120 (March), 312–321. https://doi.org/10.1016/j.foodres.2019.03.003.
[55] Rocchetti, G., Zhang, L., Bocchi, S., Giuberti, G., Ak, G., Elbasan, F., et al., 2022. The functional potential of nine Allium species related to their untargeted phytochemical characterization, antioxidant capacity and enzyme inhibitory ability. Food Chem 368 (June 2021), 130782. https://doi.org/10.1016/j.foodchem.2021.130782.
[56] Rohart, F., Gautier, B., Singh, A., Lê Cao, K.A., 2017. mixOmics: an R package for 'omics feature selection and multiple data integration. PLoS Comput Biol 13 (11), 1–19. https://doi.org/10.1371/journal.pcbi.1005752.
[57] EFSA Panel on Food Contact Materials, Enzymes, Flavourings and Processing Aids (CEF), 2016. Safety assessment of the substance zinc oxide, nanoparticles, for use in food contact materials. EFSA J 14 (3). https://doi.org/10.2903/j.efsa.2016.4408.
[58] Schloss, P.D., Westcott, S.L., Ryabin, T., Hall, J.R., Hartmann, M., Hollister, E.B., et al., 2009. Introducing mothur: open-source, platform-independent, community-supported software for describing and comparing microbial communities. Appl Environ Microbiol 75 (23), 7537–7541. https://doi.org/10.1128/AEM.01541-09.
[59] EFSA Panel on Food Additives and Nutrient Sources added to Food (ANS), 2016. Scientific opinion on the re-evaluation of silver (E 174) as food additive. EFSA J 14 (1). https://doi.org/10.2903/j.efsa.2016.4364.
[60] Scott, S.A., Fu, J., Chang, P. v, 2020. Microbial tryptophan metabolites regulate gut barrier function via the aryl hydrocarbon receptor. Proc Natl Acad Sci USA 117 (32), 19376–19387. https://doi.org/10.1073/pnas.2000047117.
[61] Scoville, E.A., Allaman, M.M., Adams, D.W., Motley, A.K., Peyton, S.C., Ferguson, S.L., et al., 2019. Serum polyunsaturated fatty acids correlate with serum cytokines and clinical disease activity in Crohn's disease. Sci Rep 9 (1), 1–11. https://doi.org/10.1038/s41598-019-39232-z.
[62] Sharon, P., Stenson, W.F., 1984. Enhanced synthesis of leukotriene B4 by colonic mucosa in inflammatory bowel disease. Gastroenterology 86 (3), 453–460. https://doi.org/10.1016/S0016-5085(84)80015-3.
[63] Shi, J.H., Axson, J.L., Bergin, I.L., Ault, A.P., 2020. Nanoparticle digestion simulator reveals pH-dependent aggregation in the gastrointestinal tract. Anal Chem 92 (18), 12257–12264. https://doi.org/10.1021/acs.analchem.0c01844.
[64] Smith, E.A., Macfarlane, G.T., 1996. Enumeration of human colonic bacteria producing phenolic and indolic compounds: effects of pH, carbohydrate availability and retention time on dissimilatory aromatic amino acid metabolism. J Appl Bacteriol 81 (3), 288–302. https://doi.org/10.1111/j.1365-2672.1996.tb04331.x.
[65] Tsugawa, H., Cajka, T., Kind, T., Ma, Y., Higgins, B., Ikeda, K., et al., 2015. MS-DIAL: data-independent MS/MS deconvolution for comprehensive metabolome analysis. Nat Methods 12 (6), 523–526. https://doi.org/10.1038/nmeth.3393.
[66] Vasileiadis, S., Puglisi, E., Arena, M., Cappa, F., van Veen, J.A., Cocconcelli, P.S., et al., 2013. Soil microbial diversity patterns of a lowland spring environment. FEMS Microbiol Ecol 86 (2), 172–184. https://doi.org/10.1111/1574-6941.12150.
[67] Wang, D., Lin, Z., Wang, T., Yao, Z., Qin, M., Zheng, S., et al., 2016. Where does the toxicity of metal oxide nanoparticles come from: the nanoparticles, the ions, or a combination of both. J Hazard Mater 308, 328–334. https://doi.org/10.1016/j.jhazmat.2016.01.066.
[68] Wang, S., Kang, X., Alenius, H., Wong, S.H., Karisola, P., El-Nezami, H., 2022. Oral exposure to Ag or TiO2 nanoparticles perturbed gut transcriptome and microbiota in a mouse model of ulcerative colitis: Ag or TiO2 nanoparticles in ulcerative colitis. Food Chem Toxicol 169 (September), 113368. https://doi.org/10.1016/j.fct.2022.113368.
[69] Wong, C.B., Odamaki, T., Xiao, J. zhong, 2019. Beneficial effects of Bifidobacterium longum subsp. longum BB536 on human health: modulation of gut microbiome as the principal action. J Funct Foods 54 (February), 506–519. https://doi.org/10.1016/j.jff.2019.02.002.

[70] Younes, M., Aquilina, G., Castle, L., Engel, K.H., Fowler, P., Frutos Fernandez, M.J., et al., 2021. Safety assessment of titanium dioxide (E171) as a food additive. EFSA J 19 (5). https://doi.org/10.2903/j.efsa.2021.6585.
[71] Kumar, R., Sahoo, S., Kian Tan, W., Kawamura, G., Matsuda, A., Kar, K.K., 2021. Microwave-assisted thin reduced graphene oxide-cobalt oxide nanoparticles as hybrids for electrode materials in supercapacitor. J. Energy Storage 40, 102724. https://doi.org/10.1016/j.est.2021.102724.
[72] Moreno-Olivas, F., Tako, E., Mahler, G.J., 2018. Retraction: ZnO nanoparticles affect intestinal function in an *in vitro* model. Food Funct. 9, 1475–1491. https://doi.org/10.1039/c8fo90013b.